Nuclear structure calculations for two-neutrino double-β decay

P. Sarriguren[1], O. Moreno[2], E. Moya de Guerra[2]
[1] *Instituto de Estructura de la Materia, IEM-CSIC, Serrano 123, E-28006 Madrid, Spain and*
[2] *Dpto. Física Atómica, Molecular y Nuclear, Univ. Complutense de Madrid, E-28040 Madrid, Spain*
(Dated: September 20, 2016)

We study the two-neutrino double-β decay in ^{76}Ge, ^{116}Cd, ^{128}Te, ^{130}Te, and ^{150}Nd, as well as the two Gamow-Teller branches that connect the double-β decay partners with the states in the intermediate nuclei. We use a theoretical microscopic approach based on a deformed selfconsistent mean field with Skyrme interactions including pairing and spin-isospin residual forces, which are treated in a proton-neutron quasiparticle random-phase approximation. We compare our results for Gamow-Teller strength distributions with experimental information obtained from charge-exchange reactions. We also compare our results for the two-neutrino double-β decay nuclear matrix elements with those extracted from the measured half-lives. Both single-state and low-lying-state dominance hypotheses are analyzed theoretically and experimentally making use of recent data from charge-exchange reactions and β decay of the intermediate nuclei.

arXiv:1609.05648v1 [nucl-th] 19 Sep 2016

I. INTRODUCTION

Double-β decay is currently one of the most studied processes both theoretically and experimentally [1–5]. It is a rare weak-interaction process of second-order taking place in cases where single β decay is energetically forbidden or strongly suppressed. It has a deep impact in neutrino physics because the neutrino properties are directly involved in the neutrinoless mode of the decay ($0\nu\beta\beta$) [6–8]. This decay mode, not yet observed, violates lepton-number conservation and its existence would be an evidence of the Majorana nature of the neutrino, providing a measurement of its absolute mass scale. Obviously, to extract a reliable estimate of the neutrino mass, the nuclear structure component of the process must be determined accurately. On the other hand, the double-β decay with emission of two neutrinos ($2\nu\beta\beta$) is perfectly allowed by the Standard Model and it has been observed experimentally in several nuclei with typical half-lives of 10^{19-21} years (see Ref. [9] for a review). Thus, to test the reliability of the nuclear structure calculations involved in the $0\nu\beta\beta$ process, one checks first the ability of the nuclear models to reproduce the experimental information available about the measured half-lives for the $2\nu\beta\beta$ process. Although the nuclear matrix elements (NME) involved in both processes are not the same, they exhibit some similarities. In particular, the two processes connect the same initial and final nuclear ground states and share common intermediate $J^\pi = 1^+$ states. Therefore, reproducing the $2\nu\beta\beta$ NMEs is a requirement for any nuclear structure model aiming to describe the neutrinoless mode.

Different theoretical approaches have been used in the past to study the $2\nu\beta\beta$ NMEs. Most of them belong to the categories of the interacting shell model [10–12], proton-neutron quasiparticle random-phase approximation (QRPA) [1, 2, 13–22], projected Hartree-Fock-Bogoliubov [23–25], and interacting boson model [26–28].

In this work we focus on the QRPA type of calculations. Most of these calculations were based originally on a spherical formalism, but the fact that some of the double-β-decay nuclei are deformed, makes it compulsory to deal with deformed QRPA formalisms [18–22]. This is particularly the case of ^{150}Nd (^{150}Sm) that has received increasing attention in the last years because of the large phase-space factor and relatively short half-life, as well as for the large $Q_{\beta\beta}$ energy that will reduce the background contamination. ^{150}Nd is currently considered as one of the best candidates to search for the $0\nu\beta\beta$ decay in the planned experiments SNO+, SuperNEMO, and DCBA.

The experimental information to constrain the calculations is not limited to the $2\nu\beta\beta$ NMEs extracted from the measured half-lives. We have also experimental information on the Gamow-Teller (GT) strength distributions of the single branches connecting the initial and final ground states with all the $J^\pi = 1^+$ states in the intermediate nucleus. The GT strength distributions have been measured in both directions from (p,n) and (n,p) charge-exchange reactions (CER) and more recently, from high resolution reactions, such as (d,^{2}He), (^{3}He,t), and (t,^{3}He) that allow us to explore in detail the low energy structure of the GT nuclear response in double-β-decay partners [29–38]. In some instances there is also experimental information on the $log(ft)$ values of the decay of the intermediate nuclei.

Nuclear structure calculations are also constrained by the experimental occupation probabilities of neutrons and protons of the relevant single-particle levels involved in the double-β-decay process. In particular, the occupation probabilities of the valence shells $1p_{3/2}, 1p_{1/2}, 0f_{5/2}$, and $0g_{9/2}$ for neutrons in ^{76}Ge and for protons in ^{76}Se have been measured in Refs. [39] and [40], respectively. The implications of these measurements on the double-β decay NMEs have been studied in Refs. [41–44].

In this paper we explore the possibility to describe all the experimental information available on the GT nuclear response within a formalism based on a deformed QRPA approach built on top of a deformed selfconsistent Skyrme Hartree-Fock calculation [45–47]. This information includes global properties about the GT resonance, such as its location and total strength, a more detailed description of the low-lying excita-

tions, and $2\nu\beta\beta$-decay NMEs. The study includes the decays ^{76}Ge $\rightarrow^{76}$Se, ^{116}Cd $\rightarrow^{116}$Sn, ^{128}Te $\rightarrow^{128}$Xe, ^{130}Te $\rightarrow^{130}$Xe, and ^{150}Nd $\rightarrow^{150}$Sm. This selection is motivated by recent high-resolution CER experiments performed for ^{76}Ge(^{3}He,t)^{76}As [36], ^{76}Se(d,^{2}He)^{76}As [34], ^{128,130}Te(^{3}He,t)^{128,130}I [38], ^{116}Cd(p,n)^{116}In and ^{116}Sn(n,p)^{116}In [37], as well as for ^{150}Nd(^{3}He,t)^{150}Pm and ^{150}Sm(t,^{3}He)^{150}Pm [35]. We also discuss on these examples the validity of the single-state dominance (SSD) hypothesis [48] and the extended low-lying-state dominance (LLSD) that includes the contribution of the low-lying excited states in the intermediate nuclei to account for the double-β-decay rates.

The paper is organized as follows: In Section II, we present a short introduction to the theoretical approach used in this work to describe the energy distribution of the GT strength. We also present the basic expressions of the $2\nu\beta\beta$-decay. In Section III we present the results obtained from our approach, which are compared with the experimental data available. Section IV contains a summary and the main conclusions.

II. THEORETICAL APPROACH

The description of the deformed QRPA approach used in this work is given elsewhere [19, 49, 50]. Here we give only a summary of the method. We start from a self-consistent deformed Hartree-Fock (HF) calculation with density-dependent two-body Skyrme interactions. Time reversal symmetry and axial deformation are assumed in the calculations [51]. Most of the results in this work are performed with the Skyrme force SLy4 [52], which is one of the most widely used and successful interactions. Results from other Skyrme interactions have been studied elsewhere [45–47, 53] to check the sensitivity of the GT nuclear response to the two-body effective interaction.

In our approach, we expand the single-particle wave functions in terms of an axially symmetric harmonic oscillator basis in cylindrical coordinates, using twelve major shells. This amounts to a basis size of 364, the total number of independent (N, n_z, λ, $\Omega > 0$) deformed H.O. states. Pairing is included in BCS approximation by solving the corresponding BCS equations for protons and neutrons after each HF iteration. Fixed pairing gap parameters are determined from the experimental mass differences between even and odd nuclei. Besides the self-consistent HF+BCS solution, we also explore the energy curves, that is, the energy as a function of the quadrupole deformation β_2, which are obtained from constrained HF+BCS calculations.

The energy curves corresponding to the nuclei studied can be found in Refs. [46, 47, 53]. The profiles of the energy curves for ^{76}Ge and ^{76}Se exhibit two shallow local minima in the prolate and oblate sectors. These minima are separated by relatively low energy barriers of about 1 MeV. The equilibrium deformation corresponds to $\beta_2 = 0.14$ in ^{76}Ge and $\beta_2 = 0.17$ in ^{76}Se. We get soft profiles for ^{116}Cd with a minimum at $\beta_2 = 0.25$ and an almost flat curve in ^{116}Sn between $\beta_2 = -0.15$ and $\beta_2 = 0.25$. We obtain almost spherical configurations in the ground states of ^{128}Te and ^{130}Te. The energies differ less than 300 keV between quadrupole deformations $\beta_2 = -0.05$ and $\beta_2 = 0.1$. On the other hand, for ^{128}Xe and ^{130}Xe we get in both cases two energy minima corresponding to prolate and oblate shapes, differing by less than 1 MeV, with an energy barrier of about 2 MeV. The ground states correspond in both cases to the prolate shapes with deformations around $\beta_2 = 0.15$. For ^{150}Nd and ^{150}Sm we obtain two energy minima, oblate and prolate, but with clear prolate ground states in both cases at $\beta_2 = 0.30$ and $\beta_2 = 0.25$, respectively. We obtain comparable results with other Skyrme forces. The relative energies between the various minima can change somewhat for different Skyrme forces [46, 47, 53], but the equilibrium deformations are very close to each other changing at most by a few percent.

After the HF+BCS calculation is performed, we introduce separable spin-isospin residual interactions and solve the QRPA equations in the deformed ground-states to get GT strength distributions and $2\nu\beta\beta$-decay NMEs. The residual force has both particle-hole (ph) and particle-particle (pp) components. The repulsive ph force determines to a large extent the structure of the GT resonance and its location. Its coupling constant χ_{ph}^{GT} is usually taken to reproduce them [49, 50, 54–56]. We use $\chi_{ph}^{GT} = 3.0/A^{0.7}$MeV. The attractive pp part is basically a proton-neutron pairing interaction. We also use a separable form [50, 55] with a coupling constant κ_{pp}^{GT} usually fitted to reproduce the experimental half-lives [56]. We use in most of this work a fixed value $\kappa_{pp}^{GT} = 0.05$ MeV, although we will explore the dependence of the $2\nu\beta\beta$ NMEs on κ_{pp}^{GT} in the next section. Earlier studies on ^{150}Nd and ^{150}Sm carried out in Refs. [21, 57] using a deformed QRPA formalism showed that the results obtained from realistic nucleon-nucleon residual interactions based on the Brueckner G matrix for the CD-Bonn force produce results in agreement with those obtained from schematic separable forces similar to those used here.

The QRPA equations are solved following the lines described in Refs. [49, 50, 55]. The method we use is as follows. We first introduce the proton-neutron QRPA phonon operator

$$\Gamma^{+}_{\omega_K} = \sum_{\pi\nu} \left[X^{\omega_K}_{\pi\nu} \alpha^{+}_{\nu} \alpha^{+}_{\bar{\pi}} + Y^{\omega_K}_{\pi\nu} \alpha_{\bar{\nu}} \alpha_{\pi} \right] , \qquad (1)$$

where α^+ and α are quasiparticle creation and annihilation operators, respectively. ω_K labels the RPA excited state and its corresponding excitation energy, and $X^{\omega_K}_{\pi\nu}, Y^{\omega_K}_{\pi\nu}$ are the forward and backward phonon amplitudes, respectively. The solution of the QRPA equations are obtained by solving first a dispersion relation [50, 55], which is of fourth order in the excitation energies ω_K. The GT transition amplitudes connecting the

QRPA ground state $|0\rangle$ ($\Gamma_{\omega_K}|0\rangle = 0$) to one phonon states $|\omega_K\rangle$ ($\Gamma^+_{\omega_K}|0\rangle = |\omega_K\rangle$) are given in the intrinsic frame by

$$\langle \omega_K|\sigma_K t^{\pm}|0\rangle = \mp M^{\omega_K}_{\pm}\,, \tag{2}$$

where

$$M^{\omega_K}_{-} = \sum_{\pi\nu}\left(v_\nu u_\pi X^{\omega_K}_{\pi\nu} + u_\nu v_\pi Y^{\omega_K}_{\pi\nu}\right)\langle \nu\,|\sigma_K|\,\pi\rangle\,, \tag{3}$$

$$M^{\omega_K}_{+} = \sum_{\pi\nu}\left(u_\nu v_\pi X^{\omega_K}_{\pi\nu} + v_\nu u_\pi Y^{\omega_K}_{\pi\nu}\right)\langle \nu\,|\sigma_K|\,\pi\rangle\,. \tag{4}$$

$v_{\nu,\pi}$ ($u^2_{\nu,\pi} = 1 - v^2_{\nu,\pi}$) are the BCS occupation amplitudes for neutrons and protons. Once the intrinsic amplitudes are calculated, the GT strength B(GT) in the laboratory frame for a transition $I_iK_i(0^+0) \to I_fK_f(1^+K)$ can be obtained as

$$B_\omega(\mathrm{GT}^{\pm}) = \sum_{\omega_K}\Big[\left\langle \omega_{K=0}\left|\sigma_0 t^{\pm}\right|0\right\rangle^2 \delta(\omega_{K=0}-\omega) + 2\left\langle \omega_{K=1}\left|\sigma_1 t^{\pm}\right|0\right\rangle^2 \delta(\omega_{K=1}-\omega)\Big]\,. \tag{5}$$

To obtain this expression we have used the Bohr and Mottelson factorization [58] to express the initial and final nuclear states in the laboratory system in terms of the intrinsic states. A quenching factor, $q = g_A/g_{A,\mathrm{bare}} = 0.79$, is applied to the weak axial-vector coupling constant and included in the calculations. The physical reasons for this quenching have been studied elsewhere [10, 59, 60] and are related to the role of non-nucleonic degrees of freedom, absent in the usual theoretical models, and to the limitations of model space, many-nucleon configurations, and deep correlations missing in these calculations. The implications of this quenching on the description of single-β and double-β-decay observables have been considered in several works [12, 27, 61–64], where both the effective value of g_A and the coupling strength of the residual interaction in the *pp* channel are considered free parameters of the calculation. It is found that very strong quenching values are needed to reproduce simultaneously the observations corresponding to the $2\nu\beta\beta$ half-lives and to the single-β decay branches. One should note however, that the QRPA calculations that require a strong quenching to fit the $2\nu\beta\beta$ NMEs were performed within a spherical formalism neglecting possible effects from deformation degrees of freedom. Because the main effect of deformation is a reduction of the NMEs, deformed QRPA calculations shall demand less quenching to fit the experiment.

Concerning the $2\nu\beta\beta$-decay NMEs, the basic expressions for this process, within the deformed QRPA formalism used in this work, can be found in Refs. [18, 19, 65]. Deformation effects on the $2\nu\beta\beta$ NMEs have also been studied within the Projected Hartree-Fock-Bogoliubov model [24]. Attempts to describe deformation effects on the $0\nu\beta\beta$ decay within QRPA models can also be found in Refs. [22, 66].

The half-life of the $2\nu\beta\beta$ decay can be written as

$$\left[T^{2\nu\beta\beta}_{1/2}\left(0^+_{\mathrm{gs}}\to 0^+_{\mathrm{gs}}\right)\right]^{-1} = (g_A)^4\, G^{2\nu\beta\beta}\,\left|(m_e c^2) M^{2\nu\beta\beta}_{GT}\right|^2\,, \tag{6}$$

where $G^{2\nu\beta\beta}$ are the phase-space integrals [67, 68] and $M^{2\nu\beta\beta}_{GT}$ the nuclear matrix elements containing the nuclear structure part involved in the $2\nu\beta\beta$ process,

$$M^{2\nu\beta\beta}_{GT} = \sum_{K=0,\pm1}\sum_{m_i,m_f}(-1)^K \frac{\langle \omega_{K,m_f}|\omega_{K,m_i}\rangle}{D} \times\langle 0_f|\sigma_{-K}t^-|\omega_{K,m_f}\rangle\,\langle \omega_{K,m_i}|\sigma_K t^-|0_i\rangle\,. \tag{7}$$

In this equation $|\omega_{K,m_i}\rangle(|\omega_{K,m_f}\rangle)$ are the QRPA intermediate 1^+ states reached from the initial (final) nucleus. m_i, m_f are labels that classify the intermediate 1^+ states that are reached from different initial $|0_i\rangle$ and final $|0_f\rangle$ ground states. The overlaps $\langle \omega_{K,m_f}|\omega_{K,m_i}\rangle$ take into account the non-orthogonality of the intermediate states. Their expressions can be found in Ref. [18]. The energy denominator D involves the energy of the emitted leptons, which is given on average by $\frac{1}{2}Q_{\beta\beta} + m_e$, as well as the excitation energies of the intermediate nucleus. In terms of the QRPA excitation energies the denominator can be written as

$$D_1 = \frac{1}{2}(\omega^{m_f}_K + \omega^{m_i}_K), \tag{8}$$

where $\omega^{m_i}_K(\omega^{m_f}_K)$ is the QRPA excitation energy relative to the initial (final) nucleus. It turns out that the NMEs are quite sensitive to the values of the denominator, especially for low-lying states, where the denominator takes smaller values. Thus, it is a common practice to use some experimental normalization of this denominator to improve the accuracy of the NMEs. In this work we also consider the denominator D_2, which is corrected with the experimental energy $\bar{\omega}_{1^+_1}$ of the first 1^+ state in the intermediate nucleus relative to the mean ground-state energy of the initial and final nuclei, in such a way that the experimental energy of the first 1^+ state is reproduced by the calculations,

$$D_2 = \frac{1}{2}\left[\omega^{m_f}_K + \omega^{m_i}_K - \left(\omega^{1_f}_K + \omega^{1_i}_K\right)\right] + \bar{\omega}_{1^+_1}\,. \tag{9}$$

Running $2\nu\beta\beta$ sums will be shown later for the two choices of the denominator D_1 and D_2. When the ground state in the intermediate nucleus of the double-β-decay partners is a 1^+ state, the energy $\bar{\omega}_{1^+_1}$ is given by

$$\bar{\omega}_{1^+_1} = \frac{1}{2}(Q_{EC} + Q_{\beta^-})_{\mathrm{exp}}\,, \tag{10}$$

TABLE I: Experimental $2\nu\beta\beta$-decay half-lives $T_{1/2}^{2\nu\beta\beta}$ from Ref. [9], phase-space factors $G^{2\nu\beta\beta}$ from Ref. [67], and NMEs extracted from Eq. (6) taking bare $g_{A,\mathrm{bare}} = 1.273$ and quenched $g_A = 1$ factors.

		^{76}Ge	^{116}Cd	^{128}Te	^{130}Te	^{150}Nd
$T_{1/2}^{2\nu\beta\beta}$ (10^{21} yr)		1.65 ± 0.14	0.0287 ± 0.0013	2000 ± 300	0.69 ± 0.13	0.0082 ± 0.0009
$G^{2\nu\beta\beta}$ (10^{-21} yr^{-1})		48.17	2764	0.2688	1529	36430
$M_{GT}^{2\nu\beta\beta}$ (MeV^{-1})	$g_A = 1.273$	0.136	0.136	0.052	0.037	0.070
	$g_A = 1$	0.220	0.220	0.084	0.060	0.113

where Q_{EC} and Q_{β^-} are the experimental energies of the decays of the intermediate nucleus into the parent and daughter partners, respectively. This is the case of ^{116}In and ^{128}I, which are both 1^+ ground states. In the other cases, although the ground state in the intermediate nuclei are not 1^+ states, the first 1^+ excited states appear at a very low excitation energy, E=0.086 MeV in ^{76}As [36], E=0.043 MeV in ^{130}I [38], and E=0.11 MeV in ^{150}Pm [35]. Therefore, to a good approximation we also determine $\bar{\omega}_{1_1^+}$ using Eq. (10).

The existing measurements for the $2\nu\beta\beta$-decay half-lives ($T_{1/2}^{2\nu\beta\beta}$) have been recently analyzed in Ref. [9]. Adopted values for such half-lives can be seen in Table I. Using the phase-space factors from the evaluation [67] that involves exact Dirac wave functions including electron screening and finite nuclear size effects, we obtain the experimental NMEs shown in Table I, for bare $g_{A,\mathrm{bare}} = 1.273$ and quenched $g_A = 1$ factors. It should be clear that the theoretical NMEs defined in Eq. (7) do not depend on the g_A factors. Hence, the value obtained for the experimental NMEs extracted from the experimental half-lives through Eq. (6) depend on the g_A value used in this equation.

III. RESULTS

A. Gamow-Teller strength distributions

The energy distributions of the GT strength obtained from our formalism are displayed in Figs. 1-2. Figure 1 contains the $B(\mathrm{GT}^-)$ strength distributions for ^{76}Ge, ^{116}Cd, ^{128}Te, ^{130}Te, and ^{150}Nd. The theoretical curves correspond to the calculated distributions folded with 1 MeV width Breit-Wigner functions, in such a way that the discrete spectra obtained in the calculations appear now as continuous curves. They give the GT strength per MeV and the area below the curves in a given energy interval gives us directly the GT strength contained in that energy interval. We compare our QRPA results from SLy4 obtained with the selfconsistent deformations with the experimental strengths extracted from CERs [31, 35, 37]. In the cases of ^{76}Ge, ^{128}Te, and ^{130}Te, the data from [31] includes the total GT measured strength of the resonances and their energy location. Namely, B(GT)=12.43 at E=11.13 MeV in ^{76}Ge, B(GT)=34.24 at E=13.14 MeV in ^{128}Te, B(GT)=38.46 at E=13.59 MeV in ^{130}Te. We have folded these strengths with the same functions used for the calculations to facilitate the comparison. They can be seen with dashed lines in Fig.1.

Figure 2 contains the $B(\mathrm{GT}^+)$ strength distributions corresponding to ^{76}Se, ^{116}Sn, ^{128}Xe, ^{130}Xe, and ^{150}Sm. The QRPA results folded with the same 1 MeV width Breit-Wigner functions are compared with the experimental strengths extracted from CERs [32–35, 37]. On the other hand, Figs. 3-4 contain the accumulated GT strength in the low excitation energy. Figure 3 contains the same cases as in Fig. 1 with additional high-resolution data from Ref. [36] for ^{76}Ge and from Ref. [38] for ^{128,130}Te. Figure 4 contains the same cases as in Fig. 2, but as accumulated strengths in the low-energy range.

One should notice that the measured strength extracted from the cross sections contains two types of contributions that cannot be disentangled, namely GT ($\sigma t^{\pm}$ operator) and isovector spin monopole (IVSM) ($r^2\sigma t^{\pm}$ operator). Thus, the measured strength corresponds actually to B(GT+IVSM). Different theoretical calculations evaluating the contributions from both GT and IVSM modes are available in the literature [35, 37, 69–71]. The general conclusion tells us that in the (p,n) direction the strength distribution below 20 MeV is mostly caused by the GT component, although non-negligible contributions from IVSM components are found between 10 and 20 MeV. Above 20 MeV, there is no significant GT strength in the calculations. In the (n,p) direction the GT strength is expected to be strongly Pauli blocked in nuclei with more neutrons than protons and therefore, the measured strength is mostly due to the IVSM resonance. Nevertheless, the strength found in low-lying

isolated peaks is associated with GT transitions because the continuous tail of the IVSM resonance is very small at these energies and is not expected to exhibit any peak. In summary, the measured strength in the (p, n) direction can be safely assigned to be GT in the low energy range below 10 MeV and with some reservations between 10 and 20 MeV. Beyond 20 MeV the strength would be practically due to IVSM. On the other hand, the measured strength in the (n, p) direction would be due to IVSM transitions, except in the low-lying excitation energy below 2-3 MeV, where the isolated peaks observed can be attributed to GT strength. This is the reason why we plot experimental data in Fig. 4 only up to 3 MeV.

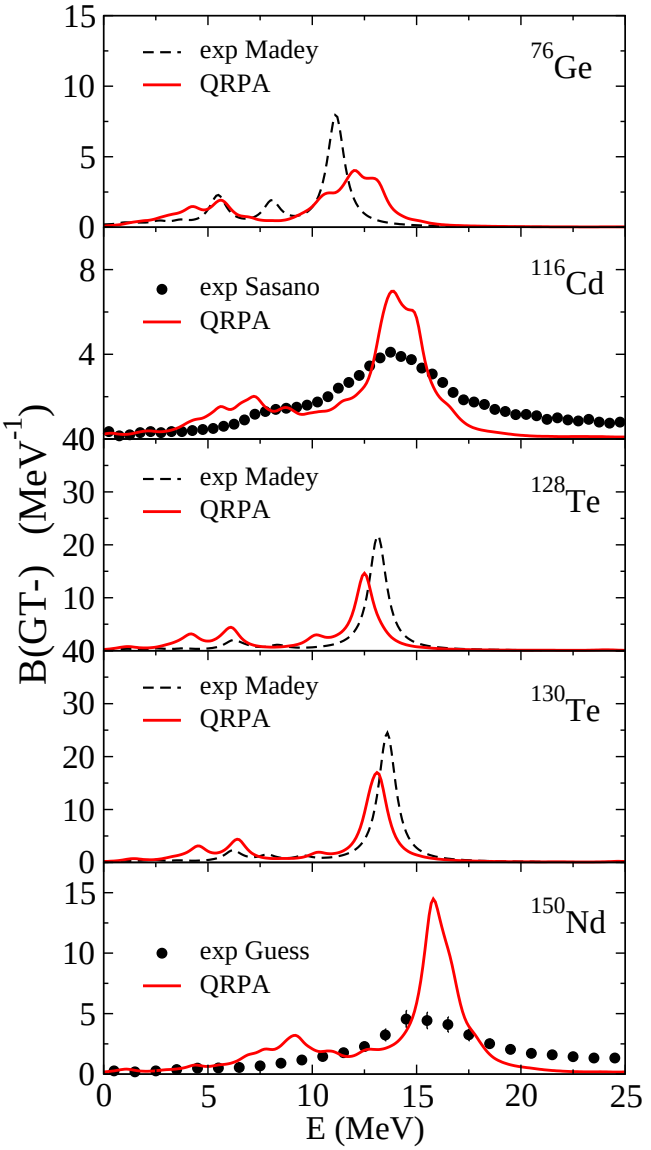

FIG. 1: Experimental $B(\mathrm{GT}^-)$ from CERs [31, 35, 37] in ^{76}Ge, ^{116}Cd, ^{128}Te, ^{130}Te, and ^{150}Nd plotted versus the excitation energy of the daughter nuclei are compared with folded SLy4-QRPA calculations (see text).

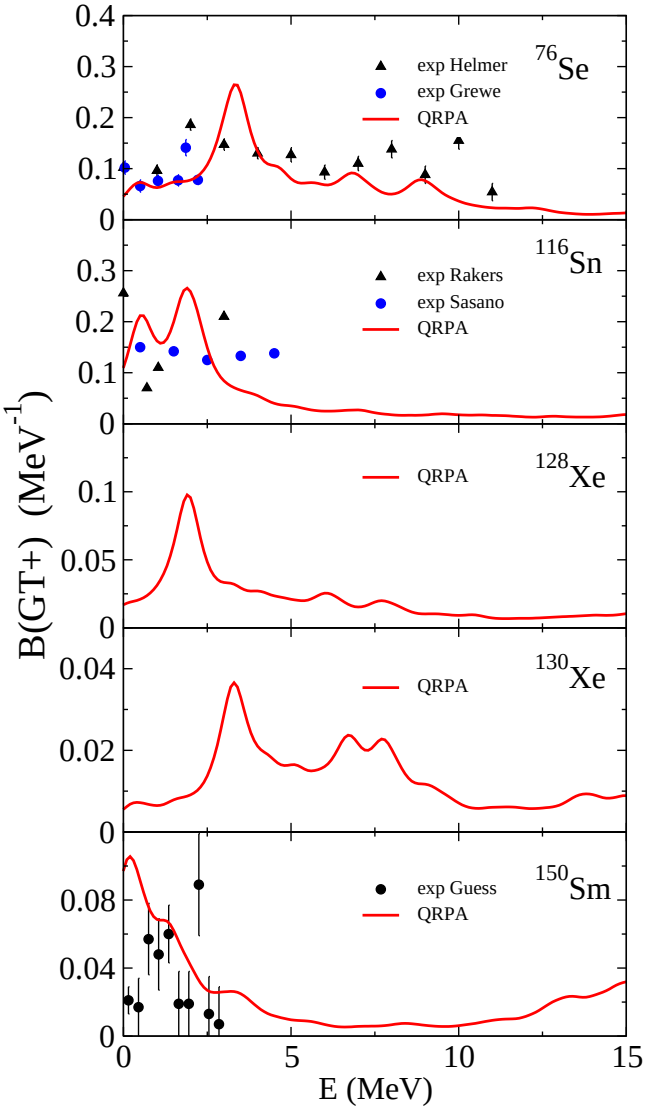

FIG. 2: Same as in Fig. 1, but for the $B(\mathrm{GT}^+)$ in ^{76}Se, ^{116}Sn, ^{128}Xe, ^{130}Xe, and ^{150}Sm. Experimental data are from CERs [32–35, 37].

In general terms, we reproduce fairly well the global properties of the GT strength distributions, including the location of the GT$^-$ resonance and the total strength measured (see Fig. 1). In the (n,p) direction, the GT$^+$ strength is strongly suppressed (compare the vertical scales in Figs. 1 and 2). As expected, a strong suppression of GT$^+$ takes place in nuclei with a large neutron excess. The experimental information on GT$^+$ strengths is mainly limited to the low-energy region and it is fairly well reproduced by the calculations. The accumulated strengths in the low-energy range shown in Figs. 3-4 show more clearly the degree of accuracy achieved by the calculations. Although a detailed spectroscopy is beyond the capabilities of our model and the isolated transitions are not well reproduced by our calculations,

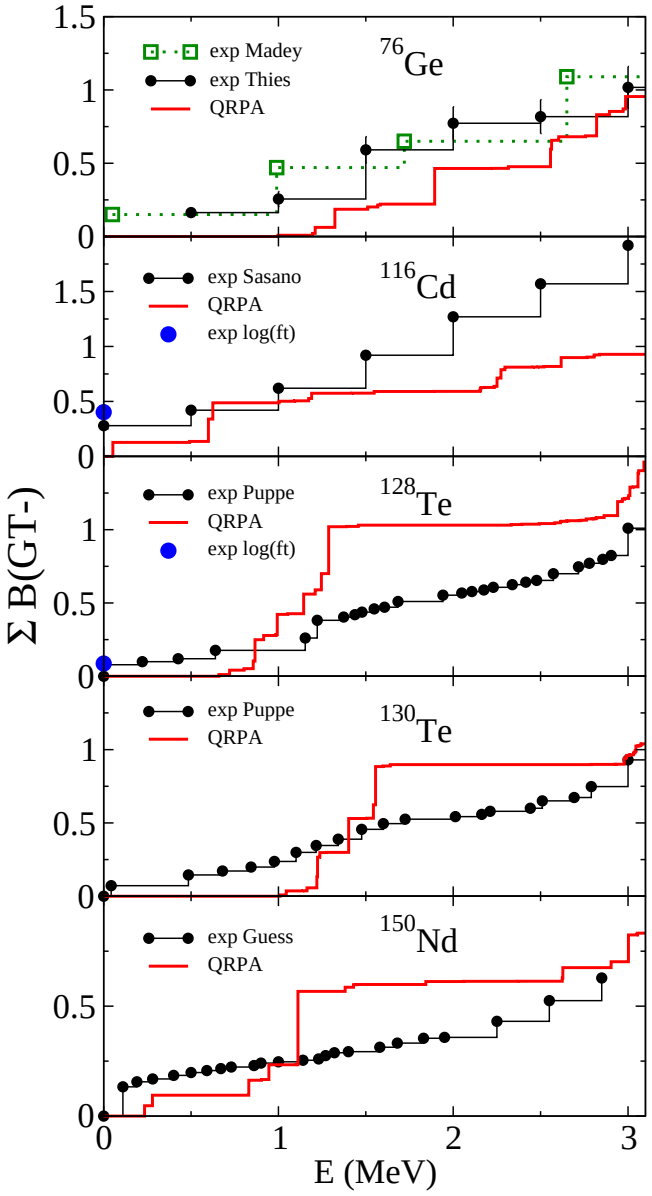

FIG. 3: Accumulated GT strength $B(\mathrm{GT}^-)$ in the low-energy range. SLy4-QRPA calculations are compared with data from Refs. [31, 35–38]. Also shown in ^{116}Cd and ^{128}Te are the $B(\mathrm{GT}^-)$ values extracted from the experimental electron captures on the intermediate nuclei ^{116}I and ^{128}In.

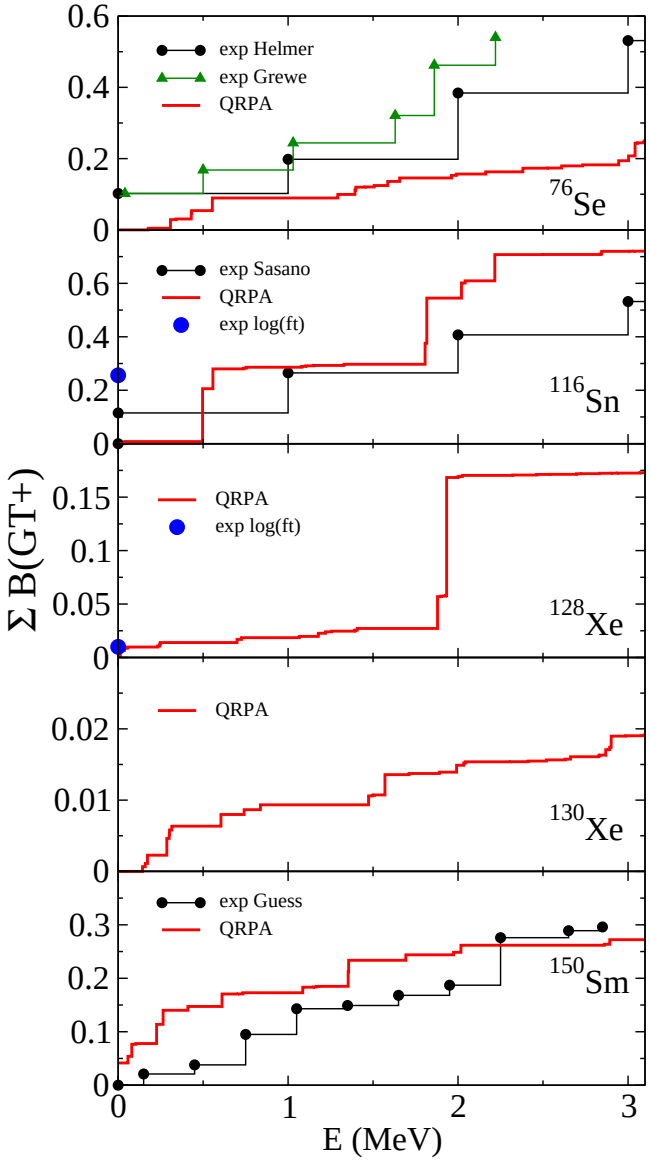

FIG. 4: Same as in Fig. 2, but plotted as accumulated strength in the low-energy range. Also shown in ^{116}Sn and ^{128}Xe are the $B(\mathrm{GT}^+)$ values extracted from the experimental β^- decay of the intermediate nuclei ^{116}I and ^{128}In.

the overall agreement with the total strength contained in this reduced energy interval, as well as with the profiles of the accumulated strength distributions, is satisfactory. In general, the experimental B(GT^-) shows spectra more fragmented than the calculated ones, but the total strength up to 3 MeV is well reproduced with the only exception of ^{116}Cd, where we obtain less strength than observed. The total measured B(GT^+) strength up to 3 MeV is especially well reproduced in the case of ^{150}Sm, whereas it is somewhat underestimated in ^{76}Se and overestimated in ^{116}Sn.

We can see in Figs. 3 and 4 with blue dots the $B(\mathrm{GT})$ values extracted from the decays of the intermediate 1^+ nuclei ^{116}In and ^{128}I. They can be compared with experimental results extracted from CERs, as well as with the theoretical calculations. The electron capture experiment on ^{116}In [72] gives $ft = 2.84 \times 10^4$ s with a corresponding strength B(GT^-)=0.402. The β^- decay yields B(GT^-)=0.256 [33]. The decay of ^{128}I yields B(GT^-)=0.087 and B(GT^+)=0.079 [38]. The sensitivity of these distributions to the effective interactions and to nuclear deformation was discussed in previous works [19, 45, 47, 53, 65]. Different calculations [18, 21, 61, 71, 73] based also on QRPA formalisms with

different degrees of sophistication agree qualitatively in the description of the single β branches of double-β-decay partners.

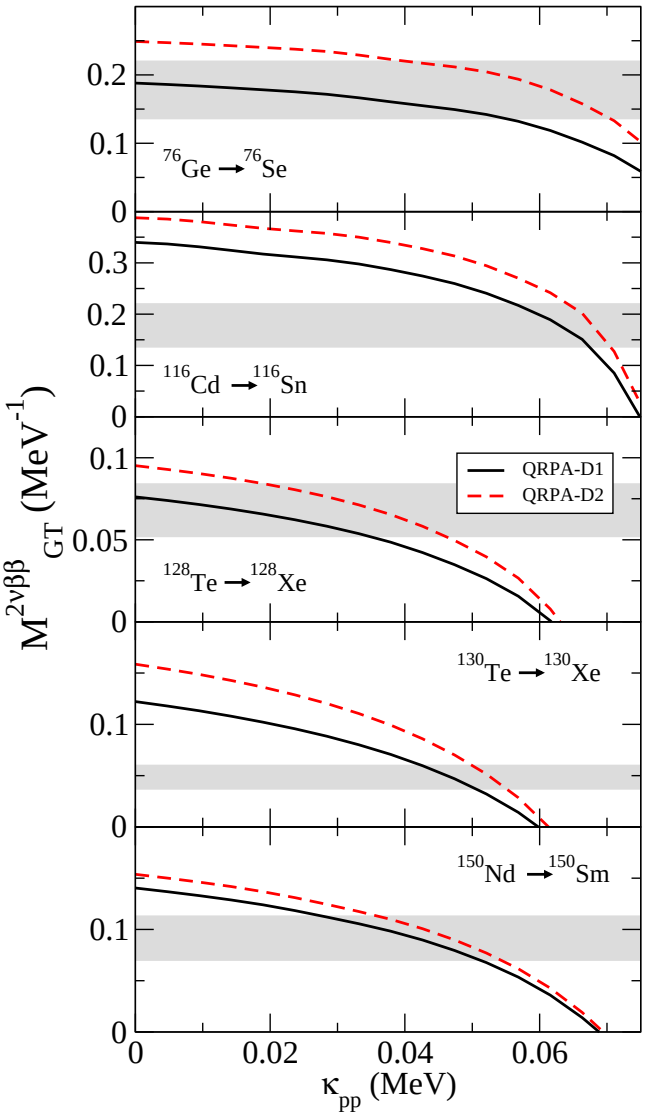

FIG. 5: Nuclear matrix element for the $2\nu\beta\beta$ decay of ^{76}Ge, ^{116}Cd, ^{128}Te, ^{130}Te, and ^{150}Nd as a function of the coupling strength κ_{pp}^{GT}. Solid lines correspond to calculations with the energy denominator D_1, while dashed lines correspond to D_2. The gray area corresponds to the NME experimental range obtained from the measured half-lives using bare $g_A = 1.273$ and quenched $g_A = 1$ factors.

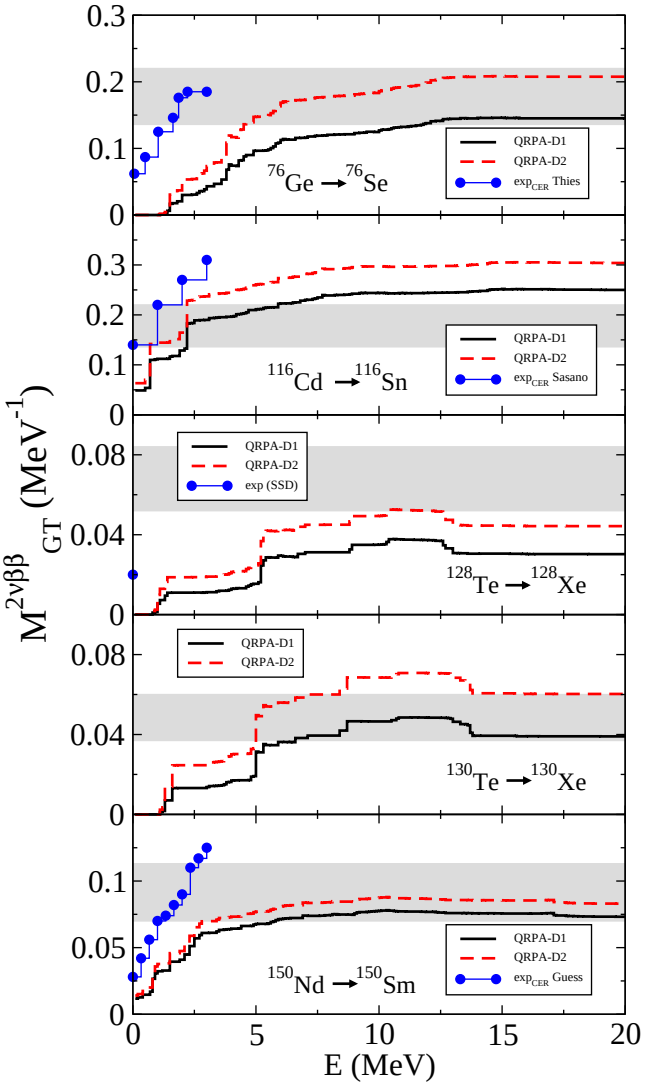

FIG. 6: Running sums of the $2\nu\beta\beta$ NME in ^{76}Ge, ^{116}Cd, ^{128}Te, ^{130}Te, and ^{150}Nd as a function of the excitation energy in the intermediate nucleus. Solid and dashed lines and shaded areas are as in Fig. 5. See text.

B. Double-β decay

It is well known that the $2\nu\beta\beta$ NMEs are very sensitive to the residual interactions, as well as to differences in deformation between initial and final nuclei [18, 19]. We show in Fig. 5 the NMEs calculated with the self-consistent deformations as a function of the pp coupling constant of the residual force for the decays of ^{76}Ge, ^{116}Cd, ^{128}Te, ^{130}Te, and ^{150}Nd. The shaded bands correspond to the experimental NMEs extracted from the measured $2\nu\beta\beta$ half-lives. For each nucleus the band is delimited by the lower and upper values obtained using bare ($g_A = 1.273$) and quenched values, respectively, (see Table I). Results obtained with the energy denominator D_1 are displayed with solid lines, whereas results obtained with D_2 are shown with dashed lines. D_2 denominators produce in all cases larger NMEs than D_1. We can see that the experimental NMEs contained in the shaded region are reproduced within some windows of the parameter κ_{pp}^{GT}. It is not our purpose here to get the best fit or the optimum value of κ_{pp}^{GT} that reproduces the experimental NMEs because this value will change

by changing χ_{ph}^{GT} or the underlying mean field structure. In this work we take $\kappa_{pp}^{GT} = 0.05$ MeV as an approximate value that reproduces reasonably well the experimental information on both single β branches and $2\nu\beta\beta$ NMEs.

Figure 6 shows the running sums for the $2\nu\beta\beta$ NMEs calculated with $\kappa_{pp}^{GT} = 0.05$ MeV. These are the partial contributions to the NMEs of all the 1^+ states in the intermediate nucleus up to a given energy. Obviously, the final values reached by the calculations at 20 MeV in Fig. 6 correspond to the values in Fig. 5 at $\kappa_{pp}^{GT} = 0.05$ MeV. The final values of the running sums for other κ_{pp}^{GT} can be estimated by looking at the corresponding κ_{pp}^{GT} values in Fig. 5. As in the previous figure, we also show the results obtained with denominators D_1 (solid) and D_2 (dashed). The main difference between them is originated at low excitation energies, where the relative effect of using shifted energies is enhanced. The effect at larger energies is negligible and we get a constant difference between D_1 and D_2, which is the difference accumulated in the first few MeV. The contribution to the $2\nu\beta\beta$ NMEs in the region between 10-15 MeV that can be seen in most cases, is due to the GT resonances observed in Fig. 1. This contribution is small because the joint effects of large energy denominators in Eq. (7) and the mismatch between the excitation energies of the GT^- and GT^+ resonances.

The running sums are very useful to discuss the extent to which the single-state-dominance hypothesis applies. This hypothesis tells us that, to a large extent, the $2\nu\beta\beta$ NMEs will be given by the transition through the ground state of the intermediate odd-odd nucleus in those cases where this ground state is a 1^+ state reachable by allowed GT transitions. One important consequence of the SSD hypothesis would be that the half-lives for $2\nu\beta\beta$ decay could be extracted accurately from simple experiments, such as single β^- and electron capture measurements of the intermediate nuclei to the 0^+ ground states of the neighbor even-even nuclei. Theoretically, the SSD hypothesis would also imply an important simplification of the calculations because to describe the $2\nu\beta\beta$ decay from ground state to ground state, only the wave function of the 1^+ ground state of the intermediate nucleus would be needed. Because not all of the double-β decaying nuclei have 1^+ ground states in the intermediate nuclei (only ^{116}In and ^{128}I in the nuclei considered here), the SSD condition is extended by considering the relative contributions of the low-lying excited states in the intermediate nuclei to the total $2\nu\beta\beta$ NMEs. This is called low-lying-single-state dominance [65] and can be studied in all $2\nu\beta\beta$ nuclei. From the results displayed in Fig. 6 we cannot establish clear evidences for SSD hypothesis from our calculations. Nevertheless, it is also worth mentioning that our NMEs calculated up to 5 MeV, already account for most of the total NME calculated up to 20 MeV. This results agrees qualitatively with other results obtained in different QRPA calculations [74, 75].

The SSD hypothesis can be tested experimentally in the decays of ^{116}Cd and ^{128}Te where the intermediate nuclei have 1^+ ground states. By measuring the two decay branches of ^{116}In and ^{128}I, the $log(ft)$ values of the ground state to ground state ($1^+ \rightarrow 0^+$) can be extracted. From these values one can obtain the GT strength,

$$B(\mathrm{GT}) = \frac{3A}{g_A^2 ft} \ , \tag{11}$$

with A=6289 s [76]. Finally the $2\nu\beta\beta$ NME within SSD is evaluated as

$$M_{GT}^{2\nu\beta\beta}(SSD) = \frac{\left[B(\mathrm{GT}^-)B(\mathrm{GT}^+)\right]^{1/2}}{(Q_{\beta^-} + Q_{\mathrm{EC}})/2} = \frac{6A}{\left[ft_{\mathrm{EC}}\right]^{1/2}\left[ft_{\beta^-}\right]^{1/2} g_A^2 (Q_{\beta^-} + Q_{\mathrm{EC}})} . \tag{12}$$

One can also determine the $2\nu\beta\beta$ NME running sums using the experimental $B(\mathrm{GT})$ extracted from CERs and using the same phases for the matrix elements if one can establish a one-to-one correspondence between the intermediate states reached from parent and daughter. Then, one can construct the $2\nu\beta\beta$ NMEs from the measured GT strengths and energies in the CERs in the parent and daughter partners,

$$M_{GT}^{2\nu\beta\beta}(LLSD) = \sum_m \frac{\left[B_m(\mathrm{GT}^+)B_m(\mathrm{GT}^-)\right]^{1/2}}{E_m + (Q_{\beta^-} + Q_{\mathrm{EC}})/2} , \tag{13}$$

where E_m is the excitation energy of the mth 1^+ state relative to the ground state of the intermediate nucleus. Experimental $2\nu\beta\beta$ NMEs running sums have been determined along this line using experimental $B(\mathrm{GT})$ from CERs in Ref. [36] for ^{76}Ge, in Ref. [37] for ^{116}Cd, and in Ref. [35] for ^{150}Nd. In the case of ^{128,130}Te they have not been determined because of the lack of data in the (n,p) direction. They can be seen in Fig. 6 under the label exp_{CER}.

In the case of ^{76}Ge, the $2\nu\beta\beta$ NMEs are constructed by combining the GT^- data from ^{76}Ge(^{3}He,t)^{76}As [36] with those for GT^+ transitions from ^{76}Se(d,^{2}He)^{76}As [34]. A large fragmentation of the GT strength was found in the experiment, not only at high excitation energies, but also at low excitation energy, which is rather unusual. In addition, a lack of correlation between the GT excitation energies from the two different branches was also observed. Thus, for the evaluation of the $2\nu\beta\beta$ NMEs a one-to-one connection between the $B(\mathrm{GT}^-)$ and $B(\mathrm{GT}^+)$ transitions leading to the excited state in the intermediate nucleus needs to be established. In particular, since the spectra from the two CER experiments had rather different energy resolutions, the strength was accumulated in similar bins to evaluate the $2\nu\beta\beta$ NMEs [36]. The summed matrix element amounted to 0.186 MeV^{-1} up to an excitation energy of 2.22 MeV.

In the case of ^{116}Cd, ^{116}Cd(p,n)^{116}In and ^{116}Sn(n,p)^{116}In [37] CERs were used to evaluate

the LLSD $2\nu\beta\beta$ NMEs. The running sum starts at 0.14 MeV^{-1} at zero excitation energy and reaches a value of 0.31 MeV^{-1} at 3 MeV excitation energy. The value at zero energy can be compared with the value obtained by using the ft-values of the decay in ^{116}In mentioned above. The value constructed in this way amounts to NME(SSD)=0.168 MeV^{-1} [72]. In the case of ^{128}Te and ^{130}Te the lack of experimental information in the GT$^+$ direction prevents us from evaluating the experimental LLSD estimates. However, an estimate of $M_{GT}^{2\nu\beta\beta}$(SSD)=0.019 MeV^{-1} in ^{128}Te can be obtained from the $log(ft)$ values of the decay in ^{128}I. Finally, in the case of ^{150}Nd, although the intermediate nucleus ^{150}Pm is not a 1^+ state, assuming that the excited 1^+ state at 0.11 MeV excitation energy observed in ^{150}Nd(^{3}He,t)^{150}Pm corresponds to all the GT strength measured between 50 keV and 250 keV in the reaction ^{150}Sm(t,^{3}He)^{150}Pm, one obtains an estimate for the SSD $M_{GT}^{2\nu\beta\beta}$(SSD)=0.028 MeV^{-1} [35]. Extending the running sum by associating the corresponding GT strengths bins from the reactions in both directions and assuming a coherent addition of all the bins, one gets $M_{GT}^{2\nu\beta\beta}$(SSD)=0.13 MeV^{-1} [35] up to an excitation energy in the intermediate nucleus of 3 MeV. This experimental running sum is included in Fig. 6. In all the cases the experimental running sum is larger than the calculations and tend to be larger than the experimental values extracted from the half-lives. However, one should always keep in mind that the present experimental LLSD estimates are indeed upper limits because the phases of the NMEs are considered always positive. Although the present calculations favor coherent phases in the low-energy region, the phases could change depending on the theoretical model. In particular the sensitivity of these phases to the pp residual interaction has been studied in Ref. [57].

IV. SUMMARY AND CONCLUSIONS

In summary, using a theoretical approach based on a deformed HF+BCS+QRPA calculation with effective Skyrme interactions, pairing correlations, and spin-isospin residual separable forces in the ph and pp channels, we have studied simultaneously the GT strength distributions of the double-β-decay partners (^{76}Ge, ^{76}Se), (^{116}Cd, ^{116}Sn), (^{128}Te, ^{128}Xe), (^{130}Te, ^{130}Xe), and (^{150}Nd, ^{150}Sm) reaching the intermediate nuclei ^{76}As, ^{116}In, ^{128}I, ^{130}I, and ^{150}Pm, respectively, as well as their $2\nu\beta\beta$ NMEs. In this work we use reasonable choices for the two-body effective interaction, residual interactions, deformations, and quenching factors. The sensitivity of the results to the various ingredients in the theoretical model was discussed elsewhere.

Our results for the energy distributions of the GT strength have been compared with recent data from CERs, whereas the calculated $2\nu\beta\beta$ NMEs have been compared with the experimental values extracted from the measured half-lives for these processes, as well as with the running sums extracted from CERs

The theoretical approach used in this work has demonstrated to be well suited to account for the rich variety of experimental information available on the nuclear GT response. The global properties of the energy distributions of the GT strength and the $2\nu\beta\beta$ NMEs are well reproduced, with the exception of a detailed description of the low-lying GT strength distributions that could clearly be improved. The $2\nu\beta\beta$ NMEs extracted from the experimental half-lives are also reproduced by the calculations with some overestimation (underestimation) in the case of ^{116}Cd (^{128}Te).

We have also upgraded the theoretical analysis of SSD and LLSD hypotheses and we have compared our calculations with the experimental running sums obtained by considering recent measurements from CERs and decays of the intermediate nuclei.

It will be interesting in the future to extend these calculations by including all the double-β-decay candidates and to explore systematically the potential of this method. It will be also interesting to explore the consequences of the isospin symmetry restoration, as it was investigated in Ref. [77]. In HF+BCS and QRPA neither the ground states nor the excited states are isospin eigenstates, but the expectation values of the T_z operator are conserved. This implies that in the $B(\mathrm{GT}^-)$ the transition operator connects states with a given expectation value of $T_z = (N-Z)/2$ to states with expectation value of $T_z = (N-Z)/2-1$.

Acknowledgments

This work was supported by MINECO (Spain) under Research Grant No. FIS2014-51971-P. O.M. acknowledges support from a Marie Curie International Outgoing Fellowship within the European Union Seventh Framework Programme, under Grant Agreement PIOF-GA-2011-298364 (ELECTROWEAK).

[1] J. Suhonen and O. Civitarese, Phys. Rep. **300**, 123 (1998).
[2] A. Faessler and F. Šimkovic, J. Phys. G: Nucl. Part. Phys. **24**, 2139 (1998).
[3] H. V. Klapdor-Kleingrothaus, *Seventy Years of Double Beta Decay*, World Scientific, Singapore (2010).
[4] O. Cremonesi and M. Pavan, Advances in High Energy Physics, vol. 2014, Article ID 951432, (2014).
[5] N. Abgrall *et al.*, Advances in High Energy Physics, vol. 2014, Article ID 365432, (2014).

[6] A. Giuliani and A. Poves, Advances in High Energy Physics, vol. 2012, Article ID 857016, (2012).
[7] J. Maalampi and J. Suhonen, Advances in High Energy Physics, vol. 2013, Article ID 505874, (2013).
[8] S. Dell'Oro, S. Marcocci, M. Viel, and F. Vissani, Advances in High Energy Physics, vol. 2016, Article ID 2162659, (2016).
[9] A. S. Barabash, Nucl. Phys. A **935**, 52 (2015).
[10] E. Caurier, G. Martinez-Pinedo, F. Nowacki, A. Poves, and A. P. Zuker, Rev. Mod. Phys. **77**, 427 (2005).
[11] J. Menéndez, A. Poves, E. Caurier, and F. Nowacki, Nucl. Phys. A **818**, 139 (2009).
[12] E. Caurier, F. Nowacki, and A. Poves, Phys. Lett. B **711**, 62 (2012).
[13] P. Vogel and M.R. Zirnbauer, Phys. Rev. Lett. **57**, 3148 (1986); D. Cha, Phys. Rev. C **27**, 2269 (1987); T. Tomoda and A. Faessler, Phys. Lett. B **199**, 475 (1987); K. Muto, E. Bender and H.V. Klapdor, Z. Phys. A **334**, 177 (1989).
[14] M. K. Cheoun, A. Bobyk, A. Faessler, F. Šimkovic, and G. Teneva, Nucl. Phys. A **561**, 74 (1993); **564**, 329 (1993).
[15] A. A. Raduta, A. Faessler, and D. S. Delion, Nucl. Phys. A **564**, 185 (1993).
[16] J. Suhonen and O. Civitarese, J. Phys. G: Nucl. Part. Phys. **39**, 085105 (2012).
[17] A. Faessler, V. Rodin, and F. Šimkovic, J. Phys. G: Nucl. Part. Phys. **39**, 124006 (2012).
[18] F. Šimkovic, L. Pacearescu, and A. Faessler, Nucl. Phys. A **733**, 321 (2004).
[19] R. Álvarez-Rodríguez, P. Sarriguren, E. Moya de Guerra, L. Pacearescu, A. Faessler, and F. Šimkovic, Phys. Rev. C **70**, 064309 (2004).
[20] A. A. Raduta, A. Escuderos, A. Faessler, E. Moya de Guerra, and P. Sarriguren, Phys. Rev. C **69**, 064321 (2004).
[21] M. S. Yousef, V. Rodin, A. Faessler, and F. Šimkovic, Phys. Rev. C **79**, 014314 (2009).
[22] M. T. Mustonen and J. Engel, Phys. Rev. C **87**, 064302 (2013).
[23] R. Chandra, J. Singh, P.K. Rath, P.K. Raina, and J.G. Hirsch, Eur. Phys. J. A **23**, 223 (2005).
[24] S. Singh, R. Chandra, P. K. Rath, P. K. Raina, and J. G. Hirsch, Eur. Phys. J. A **33**, 375 (2007).
[25] T. R. Rodríguez and G. Martínez-Pinedo, Phys. Rev. Lett. **105**, 252503 (2010).
[26] J. Barea and F. Iachello, Phys. Rev. C **79**, 044301 (2009).
[27] J. Barea, J. Kotila, and F. Iachello, Phys. Rev. C **87**, 014315 (2013).
[28] N. Yoshida and F. Iachello, Prog. Theor. Exp. Phys. 2013, 043D01.
[29] Y. Fujita, B. Rubio, and W. Gelletly, Prog. Part. Nucl. Phys. **66**, 549 (2011).
[30] D. Frekers, P. Puppe, J. H. Thies, and H. Ejiri, Nucl. Phys. A **916**, 219 (2013).
[31] R. Madey *et al.*, Phys. Rev. C **40**, 540 (1989).
[32] R.L. Helmer *et al.*, Phys. Rev. C **55**, 2802 (1997).
[33] S. Rakers *et al.*, Phys. Rev. C **71**, 054313 (2005).
[34] E.-W. Grewe *et al.*, Phys. Rev. C **78**, 044301 (2008).
[35] C. J. Guess *et al.*, Phys. Rev. C **83**, 064318 (2011).
[36] J.H. Thies *et al.*, Phys. Rev. C **86**, 014304 (2012).
[37] M. Sasano *et al.*, Phys. Rev. C **85**, 061301(R) (2012).
[38] P. Puppe *et al.*, Phys. Rev. C **86**, 044603 (2012).
[39] J.P. Schiffer *et al.*, Phys. Rev. Lett. **100**, 112501 (2008).
[40] B.P. Kay *et al.*, Phys. Rev. C **79**, 021301(R) (2009).
[41] J. Suhonen, O. Civitarese, Phys. Lett. B **668**, 277 (2008).
[42] F. Šimkovic, A. Faessler, and P. Vogel, Phys. Rev. C **79**, 015502 (2009).
[43] J. Menéndez, A. Poves, E. Caurier, and F. Nowacki, Phys. Rev. C **80**, 048501 (2009).
[44] O. Moreno, E. Moya de Guerra, P. Sarriguren, and A. Faessler, Phys. Rev. C **81**, 041303(R) (2010).
[45] P. Sarriguren, Phys. Rev. C **79**, 044315 (2009); Phys. Rev. C **86**, 034335 (2012).
[46] P. Sarriguren, O. Moreno, and E. Moya de Guerra, Rom. J. Phys. **58**, 1242 (2013).
[47] D. Navas-Nicolás and P. Sarriguren, Phys. Rev. C **91**, 024317 (2015).
[48] J. Abad, A. Morales, R. Nuñez-Lagos, and A. F. Pacheco, An. Fis. A **80**, 9 (1984).
[49] P. Sarriguren, E. Moya de Guerra, A. Escuderos, and A. C. Carrizo, Nucl. Phys. A **635**, 55 (1998); P. Sarriguren, E. Moya de Guerra, and A. Escuderos, Nucl. Phys. A **658**, 13 (1999).
[50] P. Sarriguren, E. Moya de Guerra, and A. Escuderos, Nucl. Phys. A **691**, 631 (2001); Phys. Rev. C **64**, 064306 (2001).
[51] D. Vautherin, Phys. Rev. C **7**, 296 (1973).
[52] A. Chabanat, P. Bonche, P. Haensel, J. Meyer, and R. Schaeffer, Nucl. Phys. A **635**, 231 (1998).
[53] P. Sarriguren, E. Moya de Guerra, L. Pacearescu, A. Faessler, F. Šimkovic and A.A. Raduta, Phys. Rev. C **67**, 044313 (2003).
[54] P. Moeller and J. Randrup, Nucl. Phys. A **514**, 1 (1990).
[55] K. Muto, E. Bender, and H. V. Klapdor, Z. Phys. A **333**, 125 (1989); K. Muto, E. Bender, T. Oda, and H. V. Klapdor-Kleingrothaus, Z. Phys. A **341**, 407 (1992).
[56] H. Homma, E. Bender, M. Hirsch, K. Muto, H. V. Klapdor-Kleingrothaus, and T. Oda, Phys. Rev. C **54**, 2972 (1996).
[57] D. Fang, A. Faessler, V. Rodin, M. S. Yousef, and F. Šimkovic, Phys. Rev. C **81**, 037303 (2010).
[58] A. Bohr and B. R. Mottelson, *Nuclear Structure*, (Benjamin, New York, 1969 and 1975), Vols. I and II.
[59] F. Osterfeld, Rev. Mod. Phys. **64**, 491 (1992).
[60] G. F. Bertsch and I. Hamamoto, Phys. Rev. C **26**, 1323 (1982).
[61] J. Suhonen and O. Civitarese, Nucl. Phys. **A 924**, 1 (2014).
[62] J. Suhonen and O. Civitarese, Phys. Lett. B **725**, 153 (2013).
[63] P. Pirinen and J. Suhonen, Phys. Rev. C **91**, 054309 (2015).
[64] A. Faessler, G. L. Fogli, E. Lisi, V. Rodin, A. M. Rotunno, and F. Šimkovic, J. Phys. G: Nucl. Part. Phys. **35**, 075104 (2008).
[65] O. Moreno, R. Álvarez-Rodríguez, P. Sarriguren, E. Moya de Guerra, F. Šimkovic, and A. Faessler, J. Phys. G: Nucl. Part. Phys. **36**, 015106 (2009).
[66] D. L. Fang, A. Faessler, V. Rodin, and F. Šimkovic, Phys. Rev. C **82**, 051301(R) (2010).
[67] J. Kotila and F. Iachello, Phys. Rev. C **85**, 034316 (2012).
[68] A. Neacsu and M. Horoi, Advances in High Energy Physics, vol. 2016, Article ID 7486712, (2016).
[69] I. Hamamoto and H. Sagawa, Phys. Rev. C **62**, 024319 (2000).

[70] D. R. Bes, O. Civitarese, and J. Suhonen, Phys. Rev. C **86**, 024314 (2012).
[71] O. Civitarese and J. Suhonen, Phys. Rev. C **89**, 044319 (2014).
[72] C. Wrede *et al.*, Phys. Rev. C **87**, 031303(R) (2013).
[73] D. S. Delion and J. Suhonen, Phys. Rev. C **91**, 054329 (2015).
[74] O. Civitarese and J. Suhonen, Phys. Rev. C **58**, 1535 (1998); Nucl. Phys. A **653**, 321 (1999).
[75] P. Domin, S. Kovalenko, F. Šimkovic and S. V. Semenov, Nucl. Phys. A **753**, 337 (2005); F. Šimkovic, P. Domin, and S. V. Semenov, J. Phys. G: Nucl. Part. Phys. **27**, 2233 (2001).
[76] J. C. Hardy and I. S. Towner, Phys. Rev. C **91**, 025501 (2015).
[77] F. Šimkovic, V. Rodin, A. Faessler, and P. Vogel, Phys. Rev. C **87**, 045501 (2013).